nature physics

SUPPLEMENTARY INFORMATION

https://doi.org/10.1038/s41567-020-0824-x

In the format provided by the authors and unedited.

Exponential suppression of bit-flips in a qubit encoded in an oscillator

Raphaël Lescanne[1,2], Marius Villiers[1,2], Théau Peronnin[3], Alain Sarlette[2], Matthieu Delbecq[1], Benjamin Huard[3], Takis Kontos[1], Mazyar Mirrahimi[2] and Zaki Leghtas[1,2,4] ✉

[1]Laboratoire de Physique de l'Ecole Normale Supérieure, ENS, Université PSL, CNRS, Sorbonne Université, Université de Paris, Paris, France. [2]QUANTIC team, INRIA de Paris, Paris, France. [3]Université Lyon, ENS de Lyon, Université Claude Bernard Lyon 1, CNRS, Laboratoire de Physique, Lyon, France. [4]Centre Automatique et Systèmes, Mines-ParisTech, PSL Research University, Paris, France. ✉e-mail: zaki.leghtas@mines-paristech.fr

Supplementary Information for: Exponential suppression of bit-flips in a qubit encoded in an oscillator

Raphaël Lescanne[1,2], Marius Villiers[1,2], Théau Peronnin[3], Alain Sarlette[2], Matthieu Delbecq[1], Benjamin Huard[3], Takis Kontos[1], Mazyar Mirrahimi[2], Zaki Leghtas[4,1,2]

[1] *Laboratoire de Physique de l'Ecole Normale Supérieure, ENS, Université PSL, CNRS, Sorbonne Université, Université Paris-Diderot, Sorbonne Paris Cité, Paris, France*

[2] *QUANTIC team, INRIA de Paris, 2 Rue Simone Iff, 75012 Paris, France*

[3] *Université Lyon, ENS de Lyon, Universitée Claude Bernard Lyon 1, CNRS, Laboratoire de Physique, F-69342 Lyon, France and*

[4] *Centre Automatique et Systèmes, Mines-ParisTech, PSL Research University, 60, bd Saint-Michel, 75006 Paris, France*

HAMILTONIAN DERIVATION

In this section, we derive the potential energy of the ATS dipole alone, and then calculate the full system Hamiltonian when the ATS mediates a non-linear coupling between the buffer and cat-qubit modes.

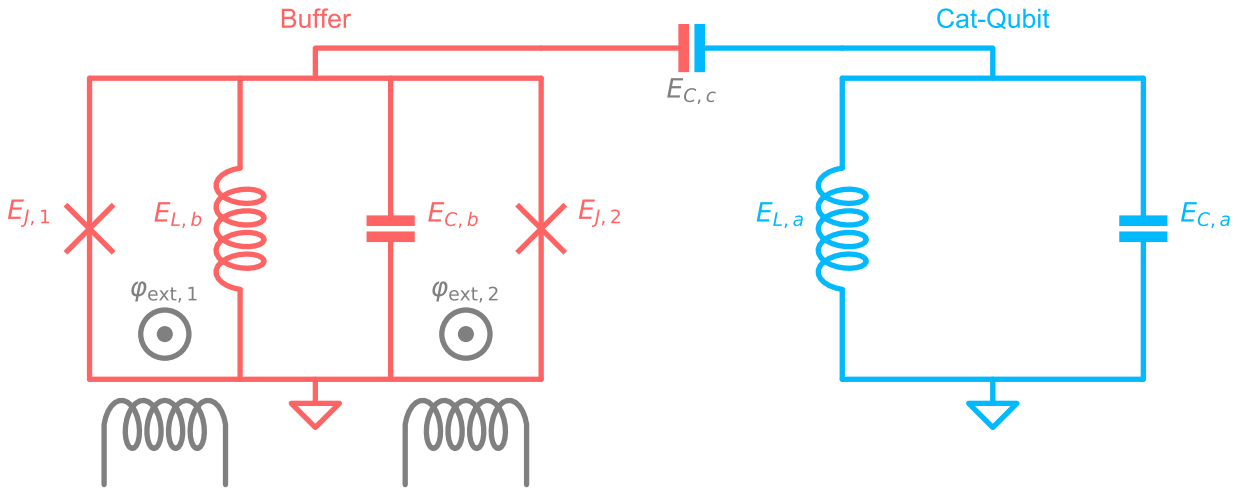

Figure S1. Equivalent circuit diagram. The cat-qubit (blue), a linear resonator, is capacitively coupled to the buffer (red). One recovers the circuit of Fig. 2 of the main text by replacing the buffer inductance with a 5-junction array and by setting $\varphi_\Sigma = (\varphi_{\text{ext},1} + \varphi_{\text{ext},2})/2$ and $\varphi_\Delta = (\varphi_{\text{ext},1} - \varphi_{\text{ext},2})/2$. Not shown here: the buffer is capacitively coupled to a transmission line, the cat-qubit resonator is coupled to a transmon qubit

The potential energy of the ATS dipole element

Let us first derive the potential energy of the ATS element alone. Its equivalent circuit is represented in red in Fig. S1 and the phase across its inductor φ is the only degree of freedom (here we assume that the coupling capacitor to the cat-qubit mode is replaced by an open circuit). The potential energy of the ATS reads

$$U(\varphi) = \frac{1}{2}E_{L,b}\varphi^2 - E_{J,1}\cos(\varphi + \varphi_{\text{ext},1}) - E_{J,2}\cos(\varphi - \varphi_{\text{ext},2}) \ . \tag{S1}$$

Due to fabrication imperfections, the ATS junctions are not symmetric. We introduce E_J and ΔE_J such that $E_{J,1} = E_J + \Delta E_J$ and $E_{J,2} = E_J - \Delta E_J$. We obtain

$$U(\varphi) = \frac{1}{2}E_{L,b}\varphi^2 - 2E_J\cos(\varphi_\Sigma)\cos(\varphi + \varphi_\Delta) + 2\Delta E_J \sin(\varphi_\Sigma)\sin(\varphi + \varphi_\Delta) \ , \tag{S2}$$

where $\varphi_\Sigma = (\varphi_{\text{ext},1} + \varphi_{\text{ext},2})/2$ and $\varphi_\Delta = (\varphi_{\text{ext},1} - \varphi_{\text{ext},2})/2$. We DC bias the ATS at the asymmetric flux bias point $\varphi_\Sigma = \varphi_\Delta = \pi/2$ (this is a saddle point of the buffer frequency map). In addition, an RF flux bias on φ_Σ is applied, so that

$$\varphi_\Sigma = \pi/2 + \epsilon(t) \ , \text{ with } \epsilon(t) = \epsilon_0\cos(\omega_p t) \tag{S3}$$

$$\varphi_\Delta = \pi/2 \ . \tag{S4}$$

The time-dependent potential at first order in $\epsilon(t)$ then reads

$$U(\varphi) = \frac{1}{2}E_{L,b}\varphi^2 - 2E_J\epsilon(t)\sin(\varphi) + 2\Delta E_J\cos(\varphi) \ . \tag{S5}$$

This potential is an unbounded function of φ, which prevents the system from escaping towards higher energy states in the presence of the pump [1, 2]. In practice, with the 5-junction array replacing the inductance, the confining part

of the potential is replaced by $5E_{J,L}\cos(\varphi/5)$ where $E_{J,L} = 5E_{L,b}$ is the Josephson energy of each individual junction of the array. This potential is no longer unbounded, however the bound is high enough ($5E_{J,L} \gg 2E_J\epsilon_0$) for our pump power regime.

In the ideal case ($\Delta E_J = 0$), this potential only produces odd powers of φ from the sine non-linearity. A small asymmetry of the junctions produces small even powers of φ, leading to parasitic Kerr non-linearities. Typically $|\Delta E_J/E_J| \approx 10\%$. In the following we assume $\Delta E_J = 0$ for simplicity.

The coupled buffer and cat-qubit resonators

We now consider the buffer and cat-qubit modes, and their coupling through the ATS dipole element. The full Hamiltonian reads

$$\boldsymbol{H} = \hbar\omega_{a,0}\boldsymbol{a}^\dagger\boldsymbol{a} + \hbar\omega_{b,0}\boldsymbol{b}^\dagger\boldsymbol{b} - 2E_J\epsilon(t)\sin\left(\boldsymbol{\varphi_b} + \boldsymbol{\varphi_a}\right) \tag{S6}$$

$$\text{with } \boldsymbol{\varphi_a} = \varphi_a(\boldsymbol{a} + \boldsymbol{a}^\dagger)\,,\ \boldsymbol{\varphi_b} = \varphi_b(\boldsymbol{b} + \boldsymbol{b}^\dagger) \tag{S7}$$

where $\boldsymbol{a}/\boldsymbol{b}$ are the annihilation operators of the cat-qubit and buffer modes, $\omega_{a/b,0}$ their resonant frequencies, and $\varphi_{a/b}$ their zero point phase fluctuations across the ATS dipole. Due to the circuit geometry, we expect $\varphi_b \gg \varphi_a$. When expanding the sine up to third order in $\boldsymbol{\varphi} = \boldsymbol{\varphi_b} + \boldsymbol{\varphi_a}$ we get

$$\begin{aligned}\boldsymbol{H} = {}& \hbar\omega_{a,0}\boldsymbol{a}^\dagger\boldsymbol{a} + \hbar\omega_{b,0}\boldsymbol{b}^\dagger\boldsymbol{b} - 2E_J\epsilon(t)\varphi_b(\boldsymbol{b} + \boldsymbol{b}^\dagger) - 2E_J\epsilon(t)\varphi_a(\boldsymbol{a} + \boldsymbol{a}^\dagger) \\ & + \frac{1}{3}E_J\epsilon(t)\left(\boldsymbol{\varphi_b} + \boldsymbol{\varphi_a}\right)^3\end{aligned} \tag{S8}$$

The first two terms of the expansion are drives at frequency ω_p on the buffer and cat-qubit respectively. They can be absorbed in the frame displaced by $\xi_a(t) = \xi_a e^{-i\omega_p t}$ and $\xi_b(t) = \xi_b e^{-i\omega_p t}$ for $\boldsymbol{a}$ and $\boldsymbol{b}$ respectively, where

$$\xi_{a/b} \xrightarrow[t\gg 1/\kappa_{a/b}]{} \frac{i(E_J/\hbar)\epsilon_0\varphi_{a/b}}{\kappa_{a/b}/2 + i(\omega_{a/b,0} - \omega_p)} \tag{S9}$$

In this displaced frame, the Hamiltonian reads

$$\begin{aligned}\boldsymbol{H}_{\text{disp}} = {}& \hbar\omega_{a,0}\boldsymbol{a}^\dagger\boldsymbol{a} + \hbar\omega_{b,0}\boldsymbol{b}^\dagger\boldsymbol{b} \\ & + \frac{1}{3}E_J\epsilon(t)\Big(\varphi_b(\boldsymbol{b} + \boldsymbol{b}^\dagger + \xi_b e^{-i\omega_p t} + \xi_b^* e^{i\omega_p t}) + \varphi_a(\boldsymbol{a} + \boldsymbol{a}^\dagger + \xi_a e^{-i\omega_p t} + \xi_a^* e^{i\omega_p t})\Big)^3\end{aligned} \tag{S10}$$

In practice, the buffer mode is driven with an additional microwave drive at frequency ω_d, not included here for simplicity. We place ourselves in the frame rotating at $(\omega_p + \omega_d)/2$ and ω_d for $\boldsymbol{a}$ and $\boldsymbol{b}$ respectively. In this rotated frame, the Hamiltonian reads

$$\begin{aligned}\boldsymbol{H}_{\text{rot}} = {}& \hbar\left(\omega_{a,0} - \frac{\omega_p + \omega_d}{2}\right)\boldsymbol{a}^\dagger\boldsymbol{a} + \hbar\left(\omega_{b,0} - \omega_d\right)\boldsymbol{b}^\dagger\boldsymbol{b} \\ & + \frac{1}{3}E_J\epsilon(t)\Big(\varphi_b(\boldsymbol{b}e^{-i\omega_d t} + \boldsymbol{b}^\dagger e^{i\omega_d t} + \xi_b e^{-i\omega_p t} + \xi_b^* e^{i\omega_p t}) + \varphi_a(\boldsymbol{a}e^{-i\frac{\omega_p+\omega_d}{2}t} + \boldsymbol{a}^\dagger e^{i\frac{\omega_p+\omega_d}{2}t} + \xi_a e^{-i\omega_p t} + \xi_a^* e^{i\omega_p t})\Big)^3\end{aligned}$$

Performing the rotating wave approximation (RWA), we get

$$\boldsymbol{H}_{\text{RWA}}/\hbar = \left(\omega_a - \frac{\omega_p + \omega_d}{2}\right)\boldsymbol{a}^\dagger\boldsymbol{a} + \left(\omega_b - \omega_d\right)\boldsymbol{b}^\dagger\boldsymbol{b} + g_2^*\boldsymbol{a}^2\boldsymbol{b}^\dagger + g_2\boldsymbol{a}^{\dagger 2}\boldsymbol{b}\,, \tag{S11}$$

where the modes frequencies are AC-Stark shifted to $\omega_{a/b} = \omega_{a/b,0} - \Delta_{a/b}$ and

$$\hbar\Delta_{a/b} = \frac{1}{3}E_J\varphi_{a/b}^2\left(\text{Re}(\xi_b)\varphi_b + \text{Re}(\xi_a)\varphi_a\right) \tag{S12}$$

with $\hbar g_2 = E_J\epsilon_0\varphi_a^2\varphi_b/2$. When we verify the frequency matching condition

$$\omega_d = \omega_b, \qquad \omega_p = 2\omega_a - \omega_b\,,$$

we recover Eq. 2 of the main text, which we recall here

$$\boldsymbol{H_i}/\hbar = g_2^*\boldsymbol{a}^2\boldsymbol{b}^\dagger + g_2\boldsymbol{a}^{\dagger 2}\boldsymbol{b}\,.$$

SEMI-CLASSICAL ANALYSIS

In this section, we compute the semi-classical dynamics of the cat-qubit resonator in the presence of various imperfections (single photon loss and detuning). We gain insight into these dynamics by introducing a pseudo-potential function. For a more complete approach, we refer the reader to Refs. [3, 4].

Two-photon dynamics

Under two-photon dissipation, the cat-qubit resonator state ρ undergoes the following dynamics

$$\frac{d}{dt}\rho = \kappa_2 D[\boldsymbol{a}^2 - \alpha^2]\rho \,, \tag{S13}$$

where the Lindblad operator D is defined for any operator $\boldsymbol{O}$ as $D[\boldsymbol{O}]\rho = \boldsymbol{O}\rho\boldsymbol{O}^\dagger - \frac{1}{2}\rho\boldsymbol{O}^\dagger\boldsymbol{O} - \frac{1}{2}\boldsymbol{O}^\dagger\boldsymbol{O}\rho$. Any combination of the states $|0,1\rangle_\alpha$ is a steady state of this dynamics. Moreover, these steady states are global attractors. To gain insight, we restrict this dynamics to the set of coherent states $\rho(t) = |\beta(t)\rangle\langle\beta(t)|$, and introduce the pseudo-potential V defined over the resonator phase space as $-\nabla V(\beta) = \frac{d\beta}{dt}$. This pseudo-potential depicts in which direction of the phase space a coherent state $|\beta\rangle$ evolves, and coherent steady states of the dynamics are the minima of V. Following ref. [5], we have

$$\frac{d\beta}{dt} = -\kappa_2\beta^*(\beta^2 - \alpha^2) \,. \tag{S14}$$

In the following we introduce $x = \mathrm{Re}(\beta)$ and $y = \mathrm{Im}(\beta)$ and we consider α real. Separating the real and imaginary part of equation (S14), we get

$$\begin{aligned}\frac{dx}{dt} &= -\kappa_2\left(x^3 + xy^2 - x\alpha^2\right)\\ \frac{dy}{dt} &= -\kappa_2\left(y^3 + yx^2 + y\alpha^2\right) \,.\end{aligned}$$

The velocity of a coherent state $|\beta\rangle$ in phase space is $(\frac{dx}{dt}, \frac{dy}{dt})$ (see Fig. S2a, S3a). By integrating this velocity over space, we get the pseudo-potential

$$V(x,y) = \kappa_2\left(\frac{1}{4}(x^4+y^4) + \frac{1}{2}x^2y^2 - \alpha^2(x^2-y^2)\right) \tag{S15}$$

depicted in Fig. 1b of the main text. It has two minima in $-\alpha$ and α. Analyzing the evolution of small deviations δx and δy around these minima, we find

$$\begin{aligned}\frac{d}{dt}\delta x &= -\kappa_{\mathrm{conf}}\delta x\\ \frac{d}{dt}\delta y &= -\kappa_{\mathrm{conf}}\delta y \,,\end{aligned}$$

where the confinement rate κ_{conf} is defined as

$$\kappa_{\mathrm{conf}} = 2\kappa_2\alpha^2 \,. \tag{S16}$$

This confinement pins down a computational state at each potential minimum, and protects the cat-qubit against errors. Next, we analyze the effect of errors on the cat-qubit resonator.

Single photon loss

When added, most Hamiltonian or dissipative mechanisms (such as detuning, single photon loss or gain, and dephasing) will perturb the system so that the two-dimensional cat-qubit space is no longer a steady-manifold of the overall dynamics. Instead, only one mixed state is a steady-state. However, this steady-state is exponentially (in $|\alpha|^2$) long to reach from the cat-qubit computational states $|0\rangle_\alpha$ and $|1\rangle_\alpha$ [3, 4]. We refer to these states as metastable

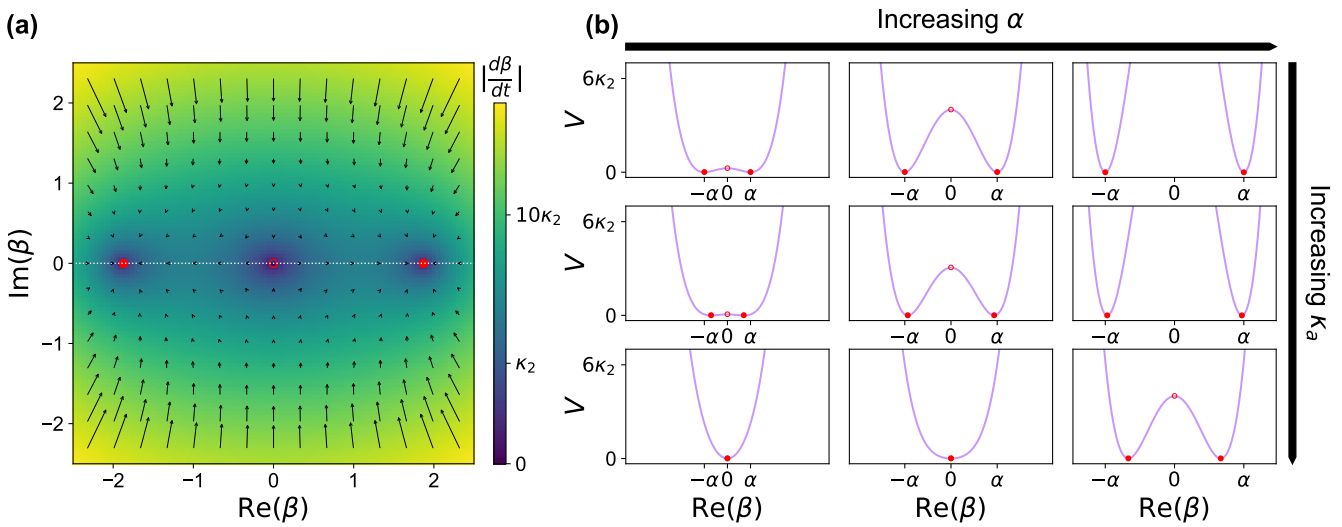

Figure S2. **Dynamics under single photon loss. (a)** This colormap represents the magnitude of the velocity field (S18) over phase space (β plane) for $\kappa_a = \kappa_2$ and $\alpha = 2$. The black arrows represent the velocity at various locations. The two stable/ one unstable steady-states are indicated with full/open red circles (the stability is infered from the direction of the arrows). The white dotted line represents the cut along which we plot the potential. **(b)** Cuts ($\mathrm{Re}(\beta) = 0$) of the potential (S19) with $\alpha = (1, 2, 3)$ (left to right) and $\kappa_a = (0, \kappa_2, 10\kappa_2)$ (top to bottom). The top row represents the unperturbed potential and the steady states are $-\alpha$ and α (red circles). As we increase κ_a, the amplitude α_∞ of the metastable states (red circles) decreases until reaching 0. However for a given value of κ_a, we can always find a value of α to recover two metastable states (bottom row).

states. We will now use the pseudo-potential representation to visulalize the main effects of single photon loss and detuning.

Let us calculate V in the presence of single photon loss at rate κ_a. The loss operator is $\boldsymbol{L}_1 = \sqrt{\kappa_a}\boldsymbol{a}$ and the overall dynamics reads

$$\frac{d}{dt}\rho = \kappa_2 D[\boldsymbol{a}^2 - \alpha^2]\rho + \kappa_a D[\boldsymbol{a}]\rho\,. \tag{S17}$$

Following the same computation as previously, we have

$$\frac{d\beta}{dt} = -\kappa_2\beta^*(\beta^2 - \alpha^2) - \frac{1}{2}\kappa_a\beta$$

so that

$$\begin{aligned}\frac{dx}{dt} &= -\kappa_2\left(x^3 + xy^2 - x\alpha^2\right) - \frac{1}{2}\kappa_a x\\ \frac{dy}{dt} &= -\kappa_2\left(y^3 + yx^2 + y\alpha^2\right) - \frac{1}{2}\kappa_a y\,.\end{aligned} \tag{S18}$$

This velocity field is represented in Fig. S2a for $\kappa_a = \kappa_2$ and $\alpha = 2$. By integrating it over space we get

$$V(x,y) = \kappa_2\left(\frac{1}{4}(x^4 + y^4) + \frac{1}{2}x^2y^2 - \alpha^2(x^2 - y^2)\right) + \frac{1}{4}\kappa_a\left(x^2 + y^2\right)\,. \tag{S19}$$

Cuts that pass through the two minima are plotted in Fig. S2b for various values of κ_a and α.

The minima of V are located in $\pm\alpha_\infty$ with

$$\alpha_\infty = \begin{cases}\sqrt{\alpha^2 - \kappa_a/(2\kappa_2)} & \text{if } \alpha^2 \geq \kappa_a/(2\kappa_2)\\ 0 & \text{otherwise}\end{cases} \tag{S20}$$

In this semi-classical analysis, we find that two metastable states form when the error rate κ_a is below the threshold

$$\kappa_a < \kappa_{\mathrm{conf}} = 2|\alpha|^2\kappa_2\,.$$

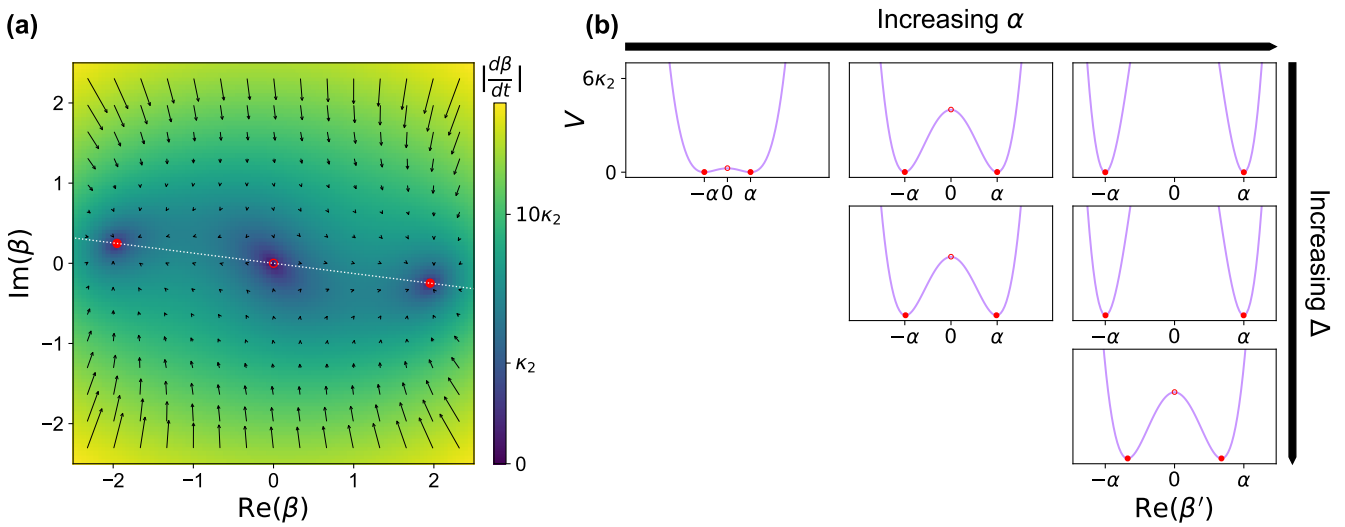

Figure S3. **Dynamics under detuning.** **(a)** This colormap represents the magnitude of the velocity field (S22) over the phase space (β plane) for $\Delta = \kappa_2$ and $\alpha = 2$. The black arrows represent the velocity at various locations. The two stable/ one unstable steady-states are indicated with full/open red circles (the stability is infered from the knowledge of the direction of the arrows). The white dotted line represents the cut along which we represent the potential. **(b)** Cuts ($\mathrm{Im}(\beta) = \lambda \mathrm{Re}(\beta)$) of the potential (S25) with $\alpha = (1, 2, 3)$ (left to right) and $\Delta = (0, \kappa_2, 8\kappa_2)$ (top to bottom). The top row represents the unperturbed potential and the steady states are $-\alpha$ and α (red circles). As we increase Δ, the amplitude $|\alpha_\infty|$ of the metastable states (red circles) decreases until reaching 0. However for a given value of Δ, we can always find a value of α to recover two metastable states (bottom row).

Detuning

In the main text, we discussed the causes of the bit-flip time saturation and blamed the random frequency shifts of the cat-qubit resonator induced by the transmon thermal excitations. Let us see how a detuning Δ of the cat-qubit frequency affects the two-photon stabilization. In this case, we have

$$\frac{d\beta}{dt} = -\kappa_2 \beta^* (\beta^2 - \alpha^2) - i\Delta\beta \tag{S21}$$

so that

$$\begin{aligned} \frac{dx}{dt} &= -\kappa_2 \left(x^3 + xy^2 - x\alpha^2\right) + \Delta y \\ \frac{dy}{dt} &= -\kappa_2 \left(y^3 + yx^2 + y\alpha^2\right) - \Delta x \,. \end{aligned} \tag{S22}$$

Note that $\mathrm{rot}(\frac{dx}{dt}, \frac{dy}{dt}) = -2\Delta \neq 0$ so we cannot perform the spatial integration to find $V(x, y)$. We can obtain the steady states directly by analyzing the velocity field (Fig. S3a) but there exists a direction in phase-space parametrized by a real parameter λ such that $y = \lambda x$ and $\frac{dy}{dt} = \lambda \frac{dx}{dt}$ along which the integration is meaningful. Plugging in this relation into (S22) we get the following condition on λ

$$\begin{aligned} \lambda^2 \Delta + 2\lambda\kappa_2\alpha^2 + \Delta &= 0 \\ \lambda = -\frac{\kappa_{\mathrm{conf}}}{2\Delta} + \sqrt{(\frac{\kappa_{\mathrm{conf}}}{2\Delta})^2 - 1} & \end{aligned} \tag{S23}$$

with $\kappa_{\mathrm{conf}} = 2\kappa_2\alpha^2$. We have chosen the solution λ which approaches 0 when $\Delta \to 0$ and for which the chosen direction crosses the steady states. Along this cut indexed by β', we have

$$\frac{d\beta'}{dt} = \left(\sqrt{\left(\frac{\kappa_{\mathrm{conf}}}{2}\right)^2 - \Delta^2}\right)\beta' - \kappa_2 \beta'^3 \tag{S24}$$

leading to

$$V(\beta') = -\frac{1}{2}\left(\sqrt{\left(\frac{\kappa_{\text{conf}}}{2}\right)^2 - \Delta^2}\right)\beta'^2 + \frac{1}{4}\kappa_2\beta'^4 \tag{S25}$$

that is plotted in Fig. S3b. There are two minima located along the direction β' in

$$|\alpha_\infty| = \begin{cases} \left(\alpha^4 - \left(\frac{\Delta}{\kappa_2}\right)^2\right)^{\frac{1}{4}} & \text{if } \Delta < \frac{\kappa_{\text{conf}}}{2} \\ 0 & \text{otherwise} \end{cases} \tag{S26}$$

In this semi-classical analysis, we find that two metastable states form provided Δ is below the threshold

$$\Delta < \kappa_{\text{conf}}/2 = |\alpha|^2\kappa_2 \ . \tag{S27}$$

In our experiment, the detuning induced by a thermal photon entering the transmon is $\Delta/2\pi = \chi/2\pi = 720\,\text{kHz}$ which is larger than $\kappa_{\text{conf}}/2/2\pi = 7\kappa_2/2\pi \approx 280\,\text{kHz}$ for the largest $|\alpha|^2 = 7$.

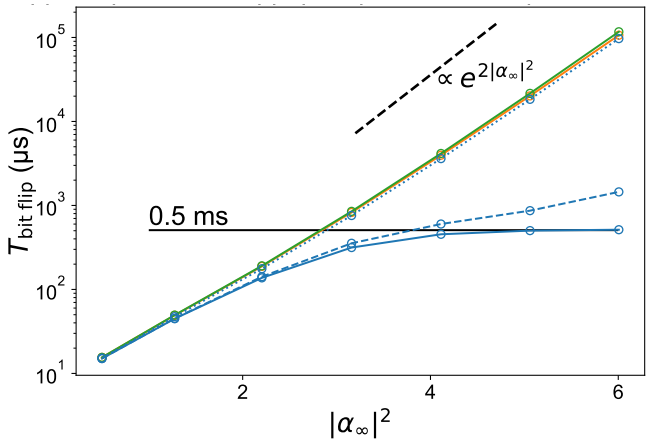

Figure S4. Simulated bit-flip time as a function of the cat-qubit size $|\alpha_\infty|^2$. We simulate the experiment displayed in Fig. 3 of the main text given the measured system parameters (Extended Data Tables 1 and 2) with a master equation solver (QuTiP) for various values of α^2. The cat-qubit size is given by $|\alpha_\infty|^2 = |\langle \boldsymbol{a}^2\rangle|$ after a time $t \gg \kappa_2^{-1}$. We simulate three models of increasing complexity: a one, two and three modes model. The green curve corresponds to the simulation of the equivalent dynamics of the cat-qubit resonator alone (S30). We get an exponential increase of the bit-flip time with a dependence on the cat size close to the theoretical prediction $\exp(2|\alpha_\infty|^2)$ [3] (dashed black line is a guide for the eye). The orange curve corresponds to the simulation of the dynamics of the buffer and cat-qubit together (S29). The good agreement between these two curves indicates that the adiabatic elimination of the buffer is valid (indeed $g_2 \ll \kappa_b$). Finally the blue solid curve is the simulation including the transmon with its thermal occupation (S28). In this case, the bit-flip time saturates at around 0.5 ms which is compatible to the experimentally measured value (1 ms). This saturation follows a prior exponential increase where the bit-flip time is multiplied by 3.7 for each added photon (experimentally 4.2). We also simulate for $\chi_{qa} = \chi_{qa,\text{exp}}/3$ (dashed blue line) and $\chi_{qa,\text{exp}}/10 = 72$ kHz (dotted blue line) and as expected, the curve approaches the exponential scaling when χ_{qa} is low enough.

BIT-FLIP TIME SIMULATION

In the previous part, we gained insight on how single photon loss and detuning affect the cat-qubit protection. In the following, we perform a full master equation simulation of the system with the measured system parameters. The system consists of three relevant modes: the buffer and cat-qubit resonator, and the transmon qubit. We can write the Hamiltonian and loss operators (in the rotating frame for each mode)

$$\boldsymbol{H_3}/\hbar = \left(g_2^*(\boldsymbol{a}^2 - \alpha^2)\boldsymbol{b}^\dagger + \text{h.c}\right) - \frac{\chi_{aa}}{2}\boldsymbol{a}^{\dagger 2}\boldsymbol{a}^2 - \chi_{qa}\boldsymbol{a}^\dagger\boldsymbol{a}\boldsymbol{q}^\dagger\boldsymbol{q} \tag{S28}$$

$$\boldsymbol{L}_a = \sqrt{\kappa_a}\boldsymbol{a},\ \boldsymbol{L}_b = \sqrt{\kappa_b}\boldsymbol{b},\ \boldsymbol{L}_q = \sqrt{\kappa_q(1+n_{\text{th}})}\boldsymbol{q},\ \boldsymbol{L}_{q^\dagger} = \sqrt{\kappa_q n_{\text{th}}}\boldsymbol{q}^\dagger$$

where we have (from left to right) in the Hamiltonian, the two-to-one photon exchange factored with a drive on the buffer with strength $\epsilon_d = -g_2^*\alpha^2$, the Kerr of the cat-qubit, the cross-Kerr between the cat-qubit and the transmon. The two last loss operators model the decay rate of the transmon (rate κ_q), and its thermal occupation measured to be $n_{th} \sim 1\%$ in the presence of the pump and drive. In order to determine the effect of the transmon on the cat-qubit, it is useful to remove the transmon from the simulation. We simulate the dynamics generated by

$$\begin{aligned} \boldsymbol{H_2}/\hbar &= \left(g_2^*(\boldsymbol{a}^2 - \alpha^2)\boldsymbol{b}^\dagger + \text{h.c}\right) - \frac{\chi_{aa}}{2}\boldsymbol{a}^{\dagger 2}\boldsymbol{a}^2 \\ \boldsymbol{L}_a &= \sqrt{\kappa_a}\boldsymbol{a},\ \boldsymbol{L}_b = \sqrt{\kappa_b}\boldsymbol{b} \end{aligned} \tag{S29}$$

Finally by adiabatically eliminating the buffer [5] we reduce to the following equivalent Hamiltonian and loss operator (provided $g_2 \ll \kappa_b$)

$$\begin{aligned} \boldsymbol{H_1}/\hbar &= -\frac{\chi_{aa}}{2}\boldsymbol{a}^{\dagger 2}\boldsymbol{a}^2 \\ \boldsymbol{L}_a &= \sqrt{\kappa_a}\boldsymbol{a},\ \boldsymbol{L}_2 = \sqrt{\kappa_2}(\boldsymbol{a}^2 - \alpha^2) \end{aligned} \tag{S30}$$

with $\kappa_2 = 4|g_2|^2/\kappa_b$.

For each of these models, we numerically solve the master equation for the cat-qubit resonator prepared in state $|+\alpha\rangle$ for various α. By fitting the decay of $\langle \boldsymbol{a} \rangle$ to an exponential decay, we extract $T_{\text{bit-flip}}$ that we reported in Fig. S4 (full lines). For the last two models, we recover the exponential increase of the bit-flip time which scales as $\sim \exp(2\alpha^2)$. The three modes model reproduces the saturation we have in the experiment and associates it with the thermal excitation of the transmon. Indeed one transmon excitation detunes the cat-qubit by χ which exceeds $\kappa_{\text{conf}}/2$ when $\alpha^2 < 18$, well above cat sizes we could achieve experimentally. In future experiment, we plan on reducing χ. By dividing χ by 10, we expect to fully circumvent this saturation (dotted lines in Fig. S4).

[1] R. Lescanne, L. Verney, Q. Ficheux, M. H. Devoret, B. Huard, M. Mirrahimi, and Z. Leghtas, "Escape of a driven quantum josephson circuit into unconfined states," *Phys. Rev. Applied*, vol. 11, p. 014030, Jan 2019.

[2] L. Verney, R. Lescanne, M. H. Devoret, Z. Leghtas, and M. Mirrahimi, "Structural instability of driven josephson circuits prevented by an inductive shunt," *Phys. Rev. Applied*, vol. 11, p. 024003, Feb 2019.

[3] J. Cohen, *Autonomous quantum error correction with superconducting qubits*. Theses, PSL Research University, Feb. 2017.

[4] M. Mirrahimi, "Quantum computation with cat qubits," *Les Houches Session, Quantum Information Machines*, 2019.

[5] Z. Leghtas, S. Touzard, I. M. Pop, A. Kou, B. Vlastakis, A. Petrenko, K. M. Sliwa, A. Narla, S. Shankar, M. J. Hatridge, M. Reagor, L. Frunzio, R. J. Schoelkopf, M. Mirrahimi, and M. H. Devoret, "Confining the state of light to a quantum manifold by engineered two-photon loss," *Science*, vol. 347, no. 6224, pp. 853–857, 2015.

[6] M. D. Reed, B. R. Johnson, A. A. Houck, L. DiCarlo, J. M. Chow, D. I. Schuster, L. Frunzio, and R. J. Schoelkopf, "Fast reset and suppressing spontaneous emission of a superconducting qubit," *Appl. Phys. Lett.*, vol. 96, p. 203110, May 2010.

[7] N. E. Frattini, V. V. Sivak, A. Lingenfelter, S. Shankar, and M. H. Devoret, "Optimizing the nonlinearity and dissipation of a snail parametric amplifier for dynamic range," *Phys. Rev. Applied*, vol. 10, p. 054020, Nov 2018.